King Saud University

Arabian Journal of Chemistry

www.ksu.edu.sa
www.sciencedirect.com

ORIGINAL ARTICLE

Improved pechini sol-gel fabrication of Li$_2$B$_4$O$_7$/NiO/Ni$_3$(BO$_3$)$_2$ nanocomposites to advanced photocatalytic performance

Makarim A. Mahdi [a], **Layth S. Jasim** [a], **Mahdi Ranjeh** [b], **Maryam Masjedi-Arani** [b], **Masoud Salavati-Niasari** [b,*]

[a] *Department of Chemistry, College of Education, University of Al-Qadisiyah, Diwaniya, Iraq*
[b] *Institute of Nano Science and Nano Technology, University of Kashan, P.O. Box 87317-51167, Kashan, Islamic Republic of Iran*

Abstract In current research, nano-scaled Li$_2$B$_4$O$_7$/NiO/Ni$_3$(BO$_3$)$_2$ (LiBNi) composites were fabricated through improved pechini sol–gel method for advanced photocatalytic applications to remove dye contaminations of drinking water under UV/Visible irradiation. To optimize LiBNi nanocomposites properties, different complexing agents including ethylenediaminetetraacetic acid (EDTA), citric acid, tannic acid, tartaric acid and phthalic acid were utilized in pechini sol–gel process. Various sizes and morphologies of Li$_2$B$_4$O$_7$/NiO/Ni$_3$(BO$_3$)$_2$ nanocomposites obtained that were characterized by SEM and TEM techniques. Also, to confirm crystalline and structural features of nano-sized LiBNi samples, analyses of X-ray diffraction (XRD), Fourier transform infrared (FT-IR) and energy dispersive X-ray (EDX) were performed. By consideration of UV–Vis data, band-gap of LiBNi nanocomposites premeditated is 3.35 eV. Moreover, photocatalytic degradation of Li$_2$B$_4$O$_7$/NiO/Ni$_3$(BO$_3$)$_2$ nanocomposites was examined via UV/visible waves in aqueous solution for degradation acid red 88 pollutant after 90 min. Some operative factors such as nanocatalyst concentration and irradiation type for optimized LiBNi nanocomposites were assessed for removal of drinking water contaminant.

1. Introduction

Nowadays, one of the important tension of the environment is the insufficiency of clean drinking water foundation due to entrance of various synthetic dye contaminations in water source from diverse industries (Sharma and Bhattacharya, 2017; Ji et al., 2021). There are numerous processes to take away non-natural dye pollutants from water source including nanofiltration (Fujioka et al., 2021; Shen et al., 2021), biosorption (Nathan et al., 2021; Ighalo and Eletta, 2020), porous adsorbent (Zhu et al., 2020; Seynnaeve et al., 2021) and UV–Vis-
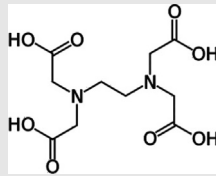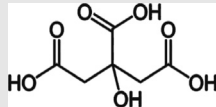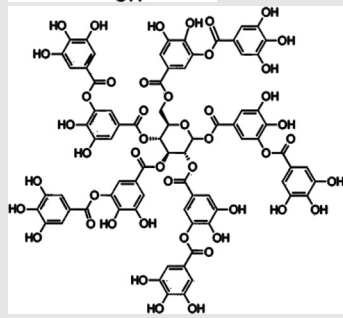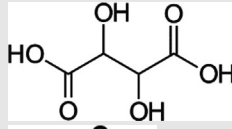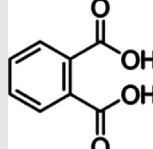
ELSEVIER **Production and hosting by Elsevier**

Table 1 Li-B-Ni nanostructures fabricated in diverse experimental conditions.

Sample	Complexing agent (CA)	EG:CA:M molar ratio	CA structures
LiBNi1	EDTA	1:1:1	
LiBNi2	Citric acid	1:1:1	
LiBNi3	Tannic acid	1:1:1	
LiBNi4	Tartaric acid	1:1:1	
LiBNi5	Phthalic acid	1:1:1	
LiBNi6	EDTA	1:0.5:1	–
LiBNi7	EDTA	1:2:1	–

ible catalytic process (Aadil et al., 2021; Wang et al., 2021). Due to low cost, low energy consumption and environmental friendly of photocatalytic degradation method, this way has been highly regarded by scientists (Saravanan et al., 2020). In UV–Visible assisted catalytic route after absorbance of UV/Visible radiation by semiconductor nanomaterials, the created electron/hole form various oxidant components of $OH^{\bullet}$, $O_2^{\bullet-}$ and H_2O_2. Finally, active components convert poisonous contamination dyes into harmless CO_2 and H_2O (Zhang et al., 2021). Recently, solid powders with suitable band gap as a semiconductor in nano scale are utilized to removal dye pollutant such as binary oxides (Mirzaei et al., 2021; Kambur et al., 2012), ternary oxide nanocomposites (Altin et al., 2021), oxyhalides (Arumugam et al., 2021; Arumugam and Choi, 2020; Arumugam et al., 2021) and carbon nanocomposites (Dashairya et al., 2021; Sayadi et al., 2021). The structural stability, chemical structure and physical properties of nano powders are significant elements for the selection of photocatalytic materials. The choice of appropriate active nanocatalyst materials and the design of an improved structure are necessary for attaining high performance in photocatalytic degradation activity. Consequently, metal oxide-supported nanomaterials with favorable bandgap as the semiconductor are crucial opportunities to design the potential active nano-catalysts. Nano-scale structure semiconductors with altered chemical compositions have been manufactured for the photocatalytic application via chemical processes include sonochemical (Masjedi-Arani and Salavati-Niasari, 2016), precipitation (Ajeesha

et al., 2021), microwave (Lu et al., 2014), pechini sol–gel method (Ranjeh et al., 2020) and hydrothermal (Guo et al., 2020) routes. In Pechini sol–gel route as an efficient method, distributed metallic ions in polymeric system including complexing agent and polyol are heated to attain promising dimensions and morphology nano-products. The pechini technique comprises creating a polymer gel by mixture of cations, polyalcohols and hydroxycarboxylic acids. Chelation and polyesterification procedures take place, then the obtained viscose gel is dried and annealed to yield oxide nanomaterials (Choura-Maatar et al., 2020). In recent years, NiO along with other semiconductor oxides has been evaluated as a photocatalyst due to ideal properties (Ma et al., 2021; Rao et al., 2021). Gue et al reported fabrication of flower-like g-C_3N_4/NiO/$Ni_3(BO_3)_2$ by thermal conversion strategy and considered photocatalytic activity for methylene blue and tetracycline removal (Guo et al., 2021). Also, Li based boron oxide nanomaterials have considered in photocatalytic process by our research team (Ranjeh et al., 2021).

The current research proposes a simple improved pechini sol–gel way to production of $Li_2B_4O_7$/NiO/$Ni_3(BO_3)_2$ (LiBNi) nanocomposite in presence of various complexing agents of EDTA, citric acid, tannic acid, tartaric acid and phthalic acid, for the first time. By alteration complexing agent type, dissimilar sizes and morphologies of nanocomposites were accomplished. Following that, photocatalytic activity of optimized $Li_2B_4O_7$/NiO/$Ni_3(BO_3)_2$ nanocomposites was investigated for removal of acid red 88 dye in waste water by UV and visible light.
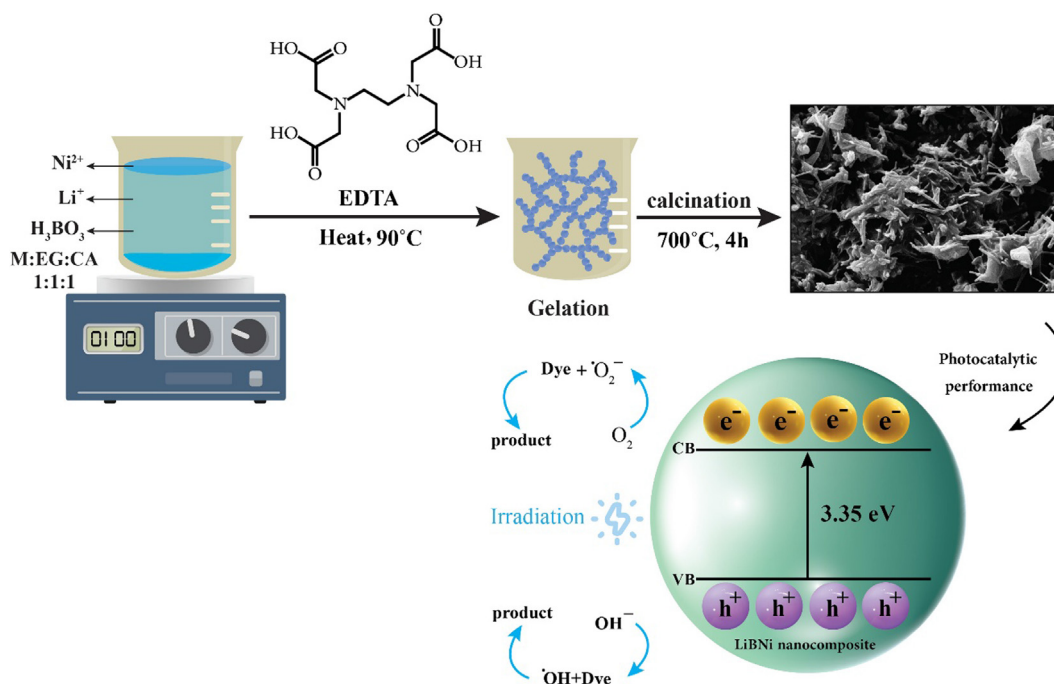
Scheme 1 Illustration plan of optimum LiBNi nano powders prepared via pechini sol–gel route in presence of EDTA complexing agent and their photocatalytic performance.

The diverse parameters such as irradiation type and nano-catalyst concentration were considered to achieving developed photocatalytic proficiency.

2. Experimental

2.1. Improved pechini sol–gel fabrication of LiBNi nanocomposites

To synthesize of Li$_2$B$_4$O$_7$/NiO/Ni$_3$(BO$_3$)$_2$ nanocomposites, starting precursors including Ni(NO$_3$)$_2$·6H$_2$O, Li$_2$CO$_3$ (Mw = 73.89 g/mol, ≥99.0%), H$_3$BO$_3$ (Mw = 61.83 g/mol), ethylene glycol (EG), EDTA, citric acid, tannic acid, tartaric acid and phthalic acid were commercially accessible and utilized without additional development. In the first step, precursors of Ni(NO$_3$)$_2$·6H$_2$O, Li$_2$CO$_3$ and H$_3$BO$_3$ were dissolved in H$_2$O and then combined together. Afterwards, ethylene glycol and complexing agent with suitable molar ratio were added to previous clear solution. After heating the final solution under magnetic stirrer at 80 °C, gel-like material is formed and following that, was placed in an oven at 90 °C for 4 h. Finally, the obtained gel sample was annealed at 700 °C for 4 h. To achieve optimum product properties for advanced photocatalytic performance, the experimental examinations carried out in different conditions. The effect of complexing agent type
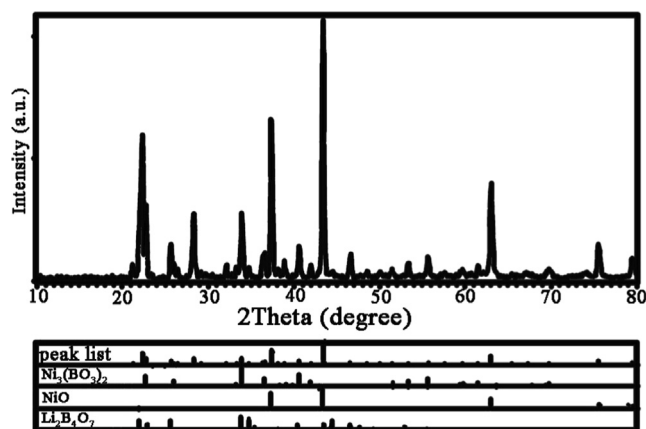

Fig. 1 XRD pattern of Li-B-Ni nanostructures fabricated through tartaric acid complexing agent (LiBNi4).

and molar ratio of ethylene glycol:complexing agent:metals precursors (EG:CA:M) was considered and the achieved data for synthesis of LiBNi nanocomposites have been resumed in Table 1. Schematic of preparation of Li$_2$B$_4$O$_7$/NiO/Ni$_3$(BO$_3$)$_2$ nanocomposites by improved pechini method has been exposed in Scheme. 1.

Table 2 The complete information about the obtained Li-B-Ni nanostructures from XRD diffractogram.

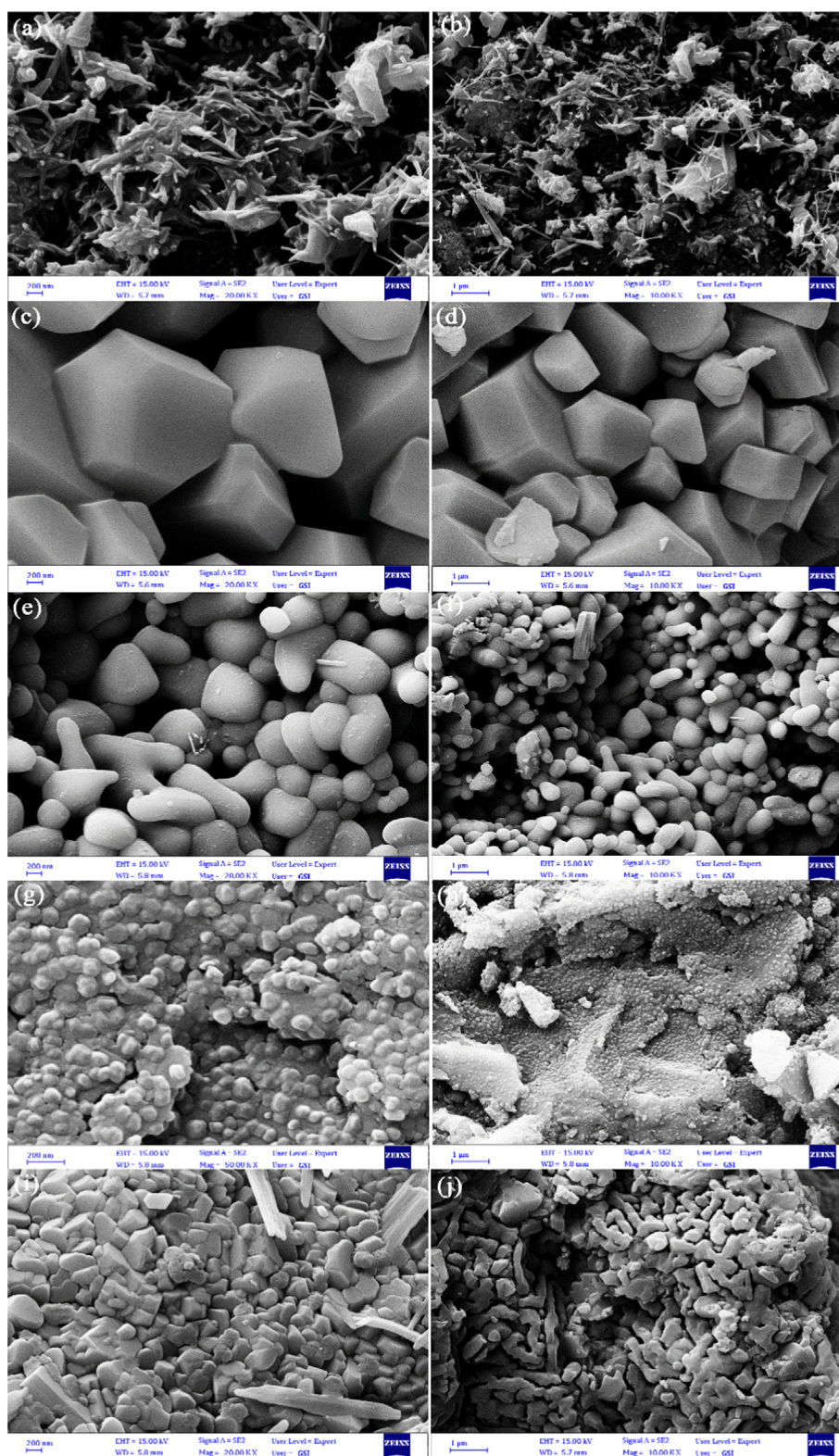| Compound	JCPDS No	Crystal phase	Space group	Cell constants (Å)		
				a	b	c
NiO	75–0197	Cubic	Fm-3m	4.1700	4.1700	4.1700
Li$_2$B$_4$O$_7$	40–0505	Tetragonal	I41cd	9.4700	9.4700	10.2790

Fig. 2 SEM nano and micrographs of Li-B-Ni nanostructures fabricated in presence of (a–j) diverse complexing agents of EDTA, citric acid, tannic acid, tartaric acid and phthalic acid, correspondingly.

2.2. UV–Visible catalytic measurements

The UV–Visible sensitive catalytic role of $Li_2B_4O_7/NiO/Ni_3(BO_3)_2$ nanocomposites was considered for removing of acid red 88 pollutant in drinking water under UV/visible radiations. According to previous works, maximum wavelength (λ_{max}) was measured 505 nm (Bankole et al., 2018). The several characters were evaluated in order to increase of
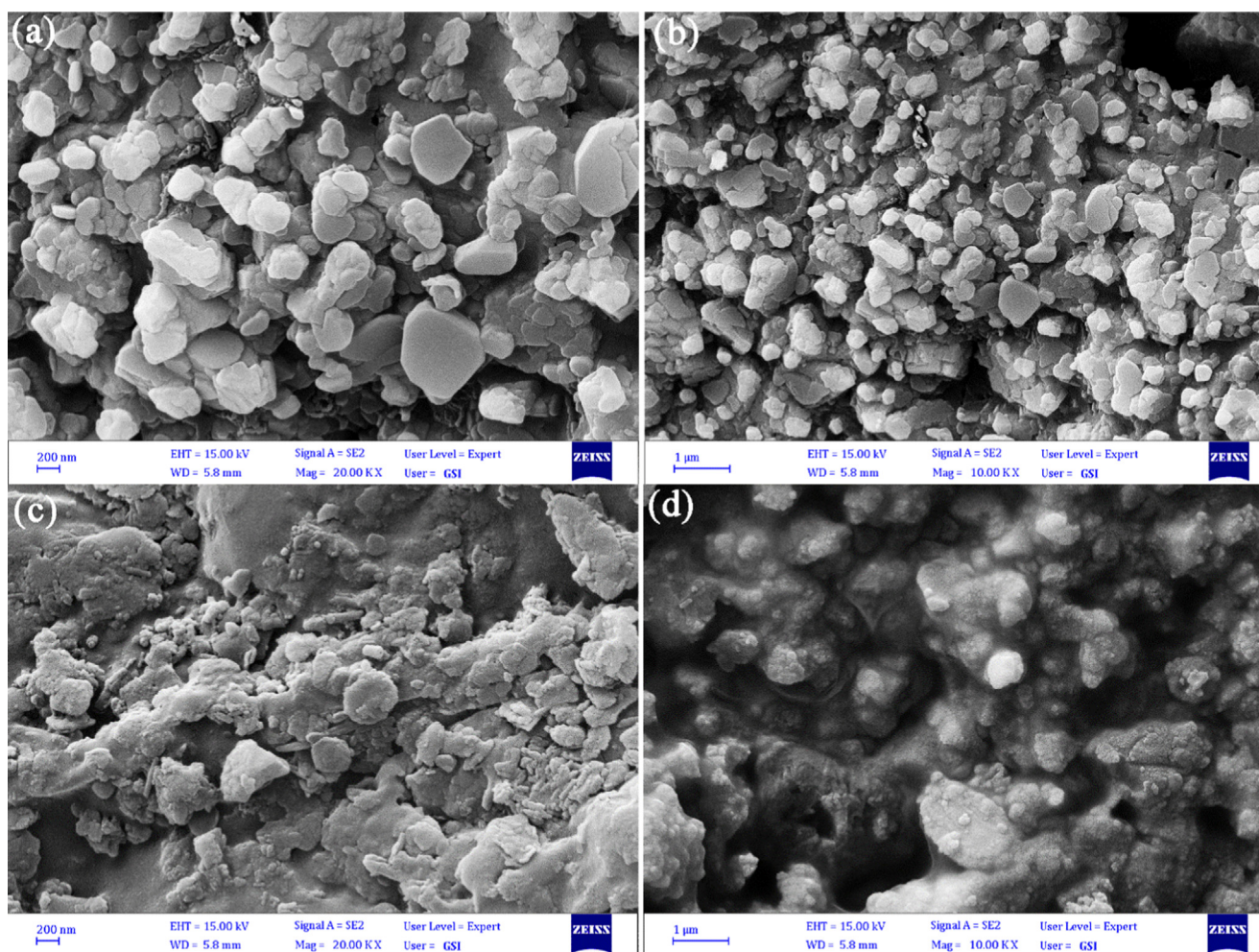
Fig. 3 SEM pictures of Li-B-Ni powder fabricated in different EG:CA:M molar ratios (a, b) 1:0.5:1 and (c, d) 1:2:1.

UV/visible-degradation efficacy including nanocatalyst concentration and irradiation category. At specific times, the absorbance of nanocomposite samples was documented by UV–Visible spectrophotometer. The UV/visible-degradation process efficiency was computed by the mentioned relation of $\eta_{photocatalytic} = [(C_0 - C_T)/C_0] * 100$ that C is concentration of solution at beginning time and after passing the defined time. UV source (Osram ULTRA-VITALUX 300 W) involving of UVA (λ: 320 to 400 nm) and UVB (λ: 290–320 nm) was used to consider photocatalytic process.

3. Results and discussion

To evaluate the crystalline phase structure of Li-B-Ni material prepared *via* improved pechini sol–gel route, XRD diffractogram of Li-B-Ni nanostructures fabricated in presence of tartaric acid complexing agent has been displayed in Fig. 1. The obtained nano sample consists of a combination of $Ni_3(BO_3)_2$, NiO and $Li_2B_4O_7$ nanocrystals. Nickel Borate ($Ni_3(BO_3)_2$) with orthorhombic crystal system and JCPDS No of 70-0956 has the main peaks at 2theta of 22.62, 25.91, 33.84, 36.48 and 40.53° related to (0 1 1), (1 1 0), (1 1 2), (1 0 3) and (2 1 1) plans, respectively. One of the other components of nanocomposite is cubic NiO (JCPDS No = 75-0197) by

three sharp peaks at 2Theta of 37.3, 43.3 and 63° associated to (1 1 1), (2 0 0) and (2 2 0) plans, correspondingly. Tetragonal Lithium Borate ($Li_2B_4O_7$) with mineral name of Diomignite (JCPDS No = 40-0505) has growth plans of (1 1 2), (0 2 2), (1 2 3), (1 3 2) and (3 3 2) related to 2θ of 21.82, 25.46, 33.64, 34.65 and 44.26°. The complete information about the achieved crystalline phases have been briefed in Table 2. Crystalline size of $Li_2B_4O_7$/NiO/$Ni_3(BO_3)_2$ (LiBNi) nanocomposite grain via Scherrer equation (Masjedi-Arani and Salavati-Niasari, 2016) was computed 36.38 nm.

One of the important factors in optimization of product morphology and size in pechini sol–gel method is changing of complexing agent. In this research, various complexing agents of EDTA, citric acid, tannic acid, tartaric acid and phthalic acid with different functional group numbers were selected. The chemical structures of all utilized chelating agents to synthesize of Li-B-Ni powder have been exhibited in Table 1. SEM nano and micrographs of Li-B-Ni nanostructures prepared in presence of diverse complexing agents of EDTA (LiBNi1), citric acid (LiBNi2), tannic acid (LiBNi3), tartaric acid (LiBNi4) and phthalic acid (LiBNi5) have been illustrated in Fig. 2a–j. As observed in Fig. 2a, b, $Li_2B_4O_7$/NiO/$Ni_3(BO_3)_2$ nanocomposites created through EDTA complexing agent have rod-like structures with length size about 100–850 nm
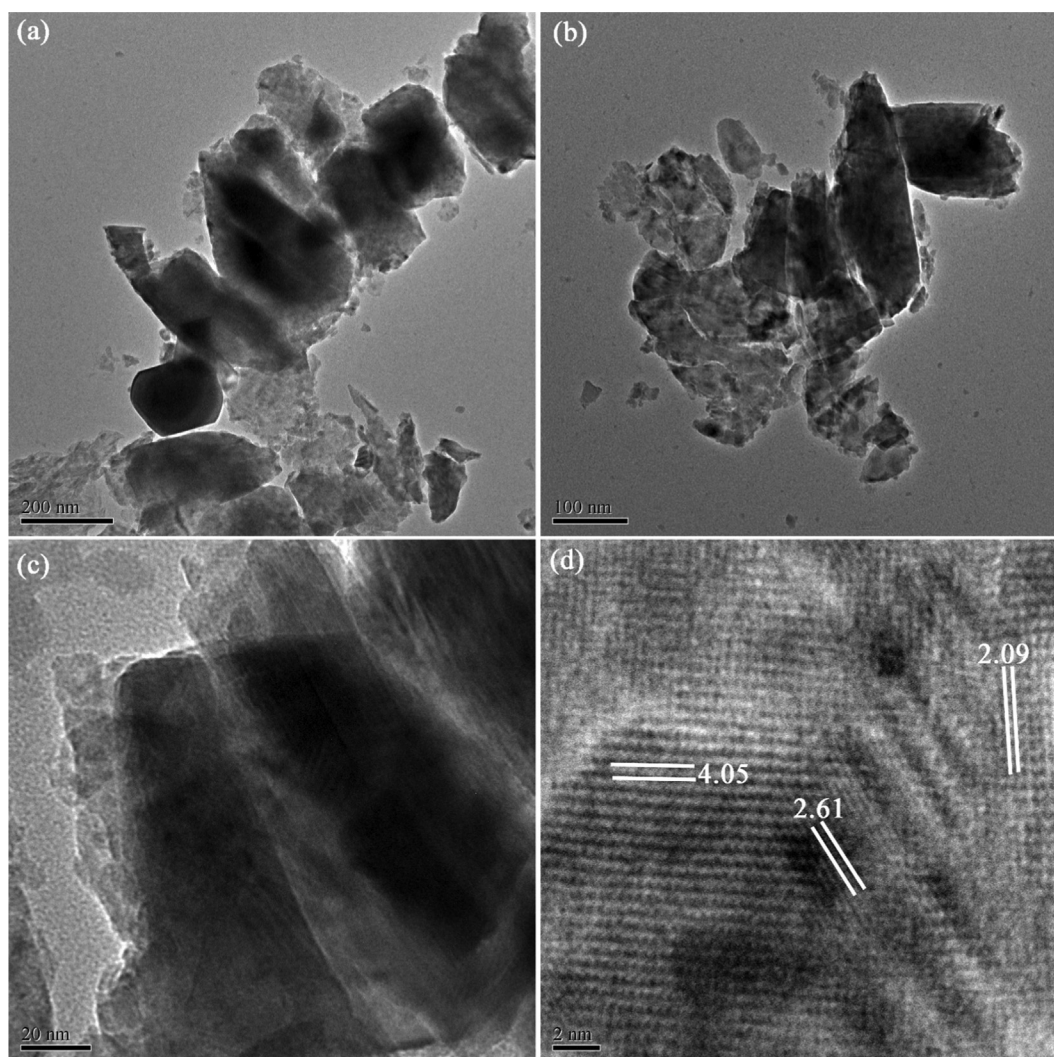
Fig. 4 (a–c) TEM and (d) HRTEM images of optimized LiBNi synthesized *via* EDTA-improved pechini sol–gel method.

and width size around 20–50 nm. LiBNi materials fabricated by citric acid are the large structures grown in different directions (size ~ 1–1.5 μm) that have been presented in Fig. 2c, d. Fig. 2e, f display spherical particles of LiBNi3 sample with approximate size of 100–800 nm that were synthesized in existing of tannic acid complexing agent. When tartaric acid was utilized as chelating agent in pechini process (LiBNi4), uniform nanoparticles with size of 40–90 nm were synthesized (Fig. 2g, h). Non-uniform structures with dissimilar morphologies and dimension were prepared with phthalic acid gelating agent (LiBNi5), that SEM pictures of them have been shown in Fig. 2i, j.

Fig. 3a–d represent SEM pictures of Li-B-Ni powders fabricated in different EG:CA:M molar ratios of 1:0.5:1 and 1:2:1, respectively. As observed in Fig. 3, decreasing or increasing of used complexing agent amounts cause the formation of agglomerated structures. The ideal EG:CA:M molar ratio is 1:1:1 that rod-like structures were fabricated (Fig. 2a, b).

TEM images of $Li_2B_4O_7/NiO/Ni_3(BO_3)_2$ (LiBNi1) nanocomposite fabricated by EDTA-improved pechini sol–gel technique in optimized experimental conditions have been displayed in Fig. 4a–c in various nano scales that the men-

tioned explanations in SEM part are confirmed. Fig. 4d demonstrates HRTEM image of LiBNi1 nanocomposite with three main planes with lattice fringe spacing of 4.05, 2.61 and 2.09 Å related to three components of nanocomposites.

FT-IR spectrum of $Li_2B_4O_7/NiO/Ni_3(BO_3)_2$ (LiBNi1) nanocomposite prepared in presence of EDTA complexing agent via improved pechini sol–gel approach has been illustrated in Fig. 5a. The wide peak around 3419 cm^{-1} and the fine peak about 1630 cm^{-1} are related to absorbed moisture by nanomaterials. The existing peaks at different cituations of 470, 621 and 999 cm^{-1} are specified to Li—O, bending vibration of B—O—B and stretching vibrating of B—O bonds, correspondingly (Ranjeh et al., 2021). A strong point positioned around 1446 cm^{-1} is associated to an unstable stretching vibration bond of BO_3 triangles and boron tetrahedral shape (Vitzthum et al., 2016; Ramteke et al., 2016). The connected water and EDTA molecules create O-H and C-O bonds around 1400–1600 cm^{-1} (Zhang et al., 2010). Also, the existing peaks around small wavenumbers of 400–600 cm^{-1} confirm attendance of M—O bonds in compounds.

The EDX profile of $Li_2B_4O_7/NiO/Ni_3(BO_3)_2$ (LiBNi1) nanocomposite arranged through improved Pechini-type
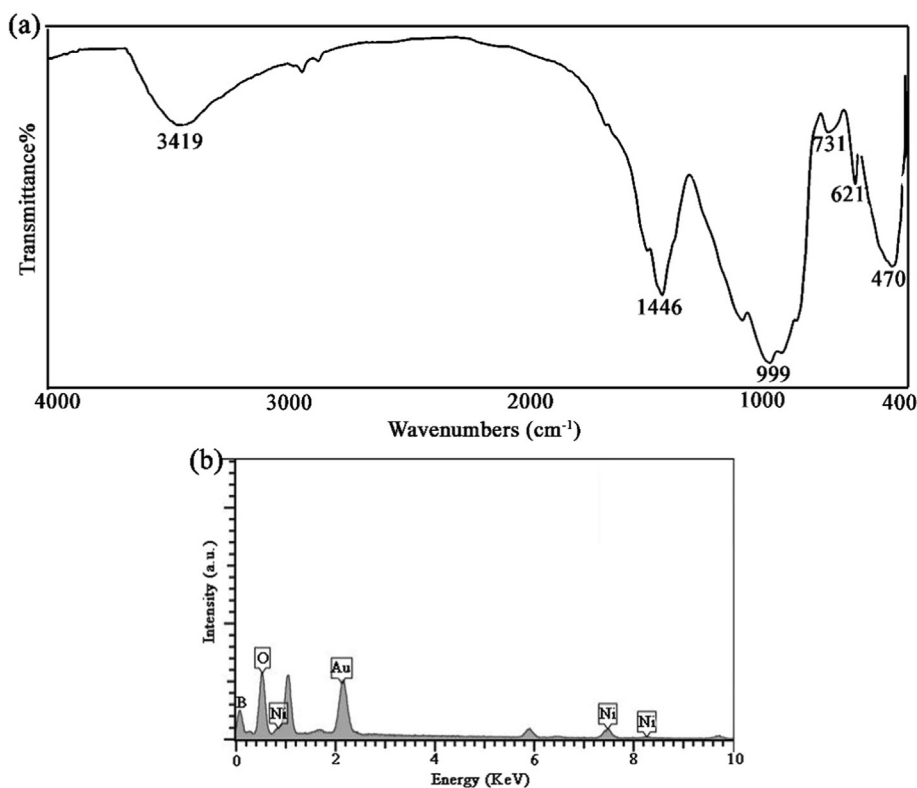
Fig. 5 (a) FT-IR spectrum and (b) EDX profile of optimized LiBNi1.

sol–gel route has been exposed in Fig. 5b. Highpoints correlated to B, Ni and O are evidently distinguished that protect formation of LiBNi nano powders.

The determination of band gap energy of nanomaterials is one the vital agents in consideration of photocatalytic activity. The UV–Vis diffuse absorption spectrum of $Li_2B_4O_7/NiO/Ni_3(BO_3)_2$ (LiBNi1) nanocomposite has been revealed in

Fig. 6. According to Tauc's relation for nano semiconductors (Tauc et al., 1966), band-gap energy of the synthesized LiBNi1 nanocomposite was determined through extrapolating of the linear segment of the plans of $(\alpha h\nu)^2$ against $h\nu$. The energy gap quantity was numerated 3.35 eV.

The magnetic possession of $Li_2B_4O_7/NiO/Ni_3(BO_3)_2$ (LiBNi1) nanocomposite using vibrating sample magnetome-
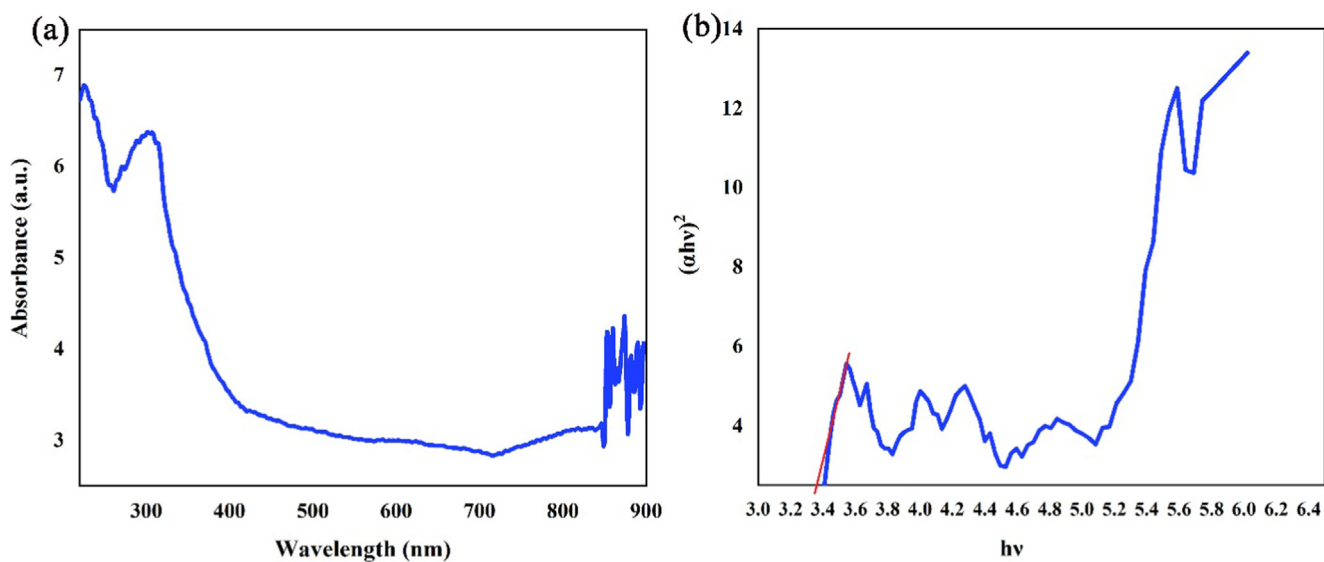

Fig. 6 (a) UV–Vis diffuse absorption spectrum and (b) linear portion of plots of $(\alpha h\nu)^2$ against $(h\nu)$ of the optimized LiBNi1 nanocomposite.
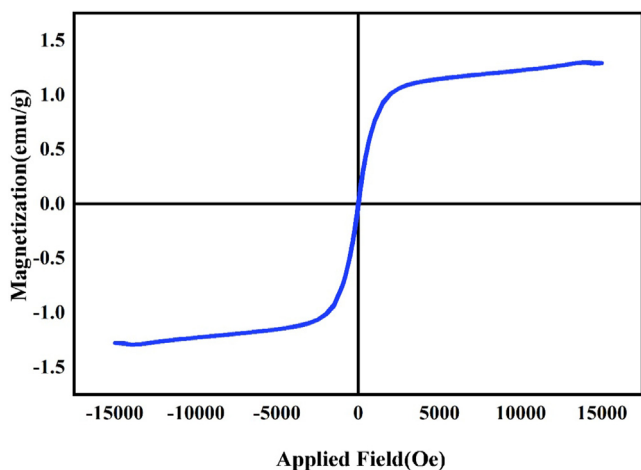
Fig. 7 Magnetization against employed magnetic field at room temperature for the optimized LiBNi1 nanocomposite.

ter (VSM) has been displayed in Fig. 7. The coercivity (Hc), supreme saturation magnetization (Ms) and residual magnetization (Mr) of developed ferromagnetic nanomaterial are about 22.71 (oersted), 1.29 (emu per g) and 0.026 (emu per g) (Ranjeh et al., 2021; Zhang et al., 2011).

According to suitable electronic structure of $Li_2B_4O_7/NiO/Ni_3(BO_3)_2$ nanocomposite components, consideration of their photocatalytic process has attracted the attention of many scientists (Guo et al., 2021). The photocatalytic tests of the optimized $Li_2B_4O_7/NiO/Ni_3(BO_3)_2$ (LiBNi1) nanocomposites were carried out in different conditions of nanocatalyst dosage of 0.02 and 0.05 g under UV and Visible radiations that the related results have been illustrated in Fig. 8. According to the obtained band gap for LiBNi1 nanocomposites, it is expected that nano sample have better photocatalytic performance under UV light than visible type. As observed in Fig. 8a, b, the photocatalytic degradation percentage of acid red 88 dye pollutant under UV irradiation in presence of 0.02 and 0.05 g $Li_2B_4O_7/NiO/Ni_3(BO_3)_2$ nanocomposites are
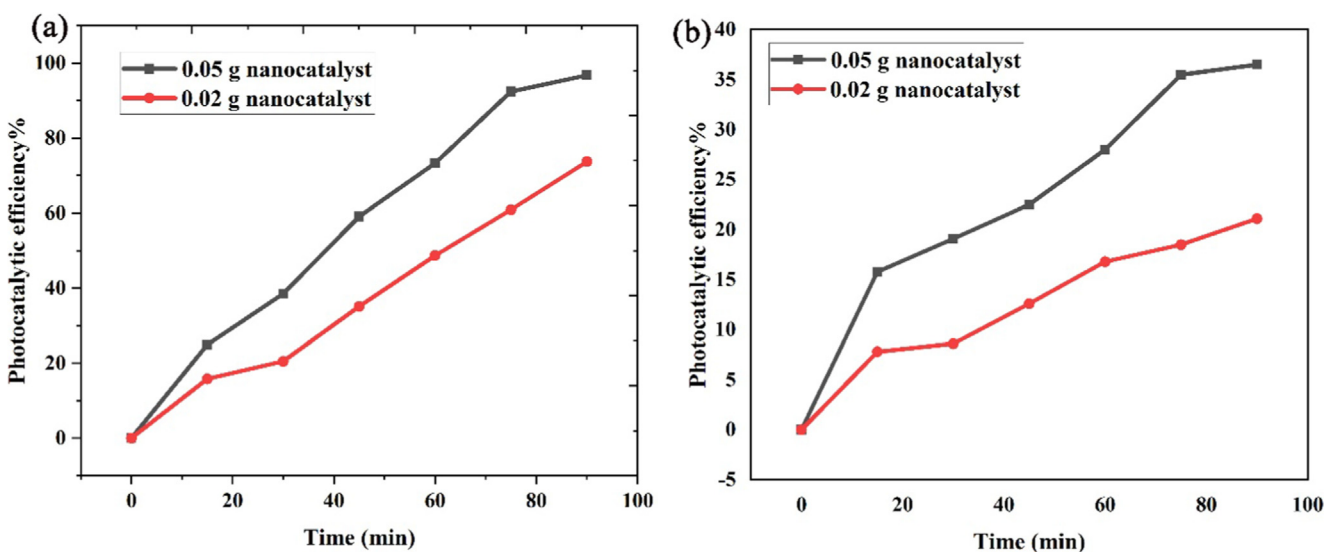

Fig. 8 Plot of pollutant degradation percentage versus reaction time of the optimized LiBNi1 nanocomposites under (a) UV and (b) visible irradiation.
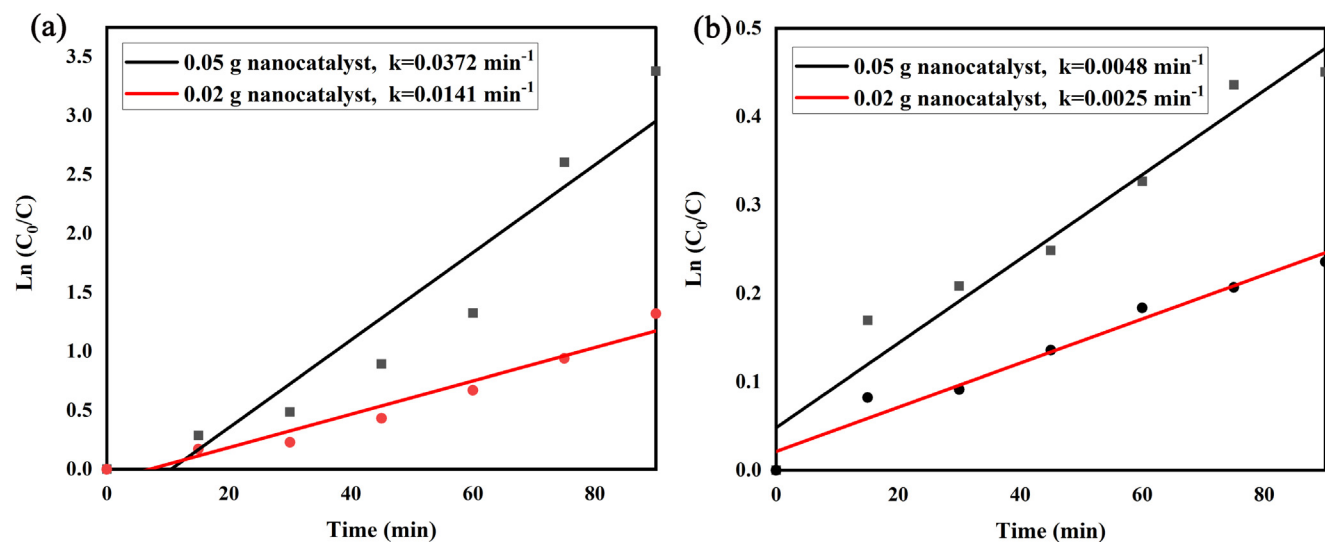

Fig. 9 Plots of $ln(C/C_0)$ vs time of the optimized LiBNi1 nanocomposites under (a) UV and (b) visible irradiation.

73.7% and 96.8%, respectively. The visible-sensitive degradation percentage of Li$_2$B$_4$O$_7$/NiO/Ni$_3$(BO$_3$)$_2$ nano-catalyst in different amounts of 0.02 and 0.05 g to remove of acid red 88 contamination after 90 min are 21.1 and 36.5%, correspondingly. From the achieved data was concluded that by increasing nano-catalyst amount in catalytic reactions, the photocatalytic performance improve.

To study the kinetic result of models matching to Langmuir–Hinshelwood technique, the capable reaction degree quantities can be extended as bellows: ln $\frac{C_0}{C_t} = kt$; Which C$_0$ and C$_t$ are acid red pollutant doping in the start and t min and k is the pseudo-1st-order degree quantity (min^{-1}) (Kim and Hong, 2002). Pursuant to linear necessities of ln(C$_0$/C$_t$) against the creation period, the first-class constant k has been achieved. According to Fig. 9a, b, the k constant for concentration of 0.05 g and UV irradiation (k = 0.0372 min^{-1}) is higher than concentration of 0.02 g and visible light (k = 0.0025 min^{-1}).

Fig. 10 displays the photo-degradation percentage of LiBNi1 nanocomposites in presence of three dissimilar scavenger mediators of Ethylenediaminetetraacetic acid (EDTA), Benzoic acid (BA) and benzoquinone (BQ) to trap h$^+$, $^\bullet$OH and $^\bullet$O$_2^-$ active specimens (Mahdiani et al., 2018; Al-Nayili and Albdiry, 2021; Kadhem and Al-Nayili, 2021; Al-Nayili, 2021), respectively for more realization of photo-degradation mechanism of acid red 88 under UV irradiation. As illustrated, the photo-degradation efficiency of acid red 88 pollutant by Li$_2$B$_4$O$_7$/NiO/Ni$_3$(BO$_3$)$_2$ nano-catalyst has noticeably reduced in presence of BA as a OH$^\bullet$ trapper. It is concluded that OH$^\bullet$ active component has the most contribution in removal dye pollutant of water. However, according to Fig. 15, $^\bullet$O$_2^-$ also plays little role in destruction of toxic dye.

To consider the repeatability of Li$_2$B$_4$O$_7$/NiO/Ni$_3$(BO$_3$)$_2$ nano-catalyst, a recycling investigation of the visible-degradation for acid red 88 pollutant was accomplished. After the first test under visible treatment, the nano-photocatalyst was separated and washed with water and acetone. The 2nd test of photocatalyst examination was done with new dye solution and previous used nanocatalyst composite. This research was repeated 5 times. As presented in Fig. 11, after 5 times
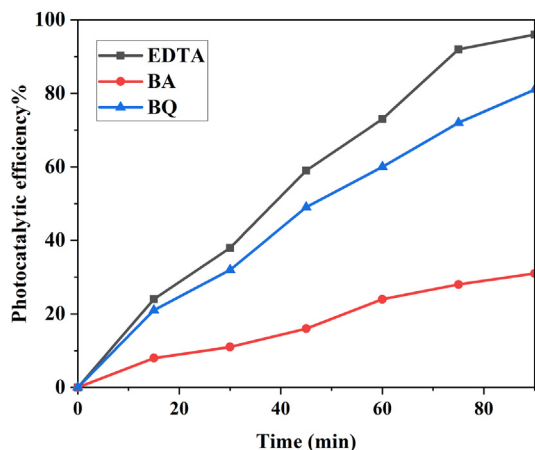

Fig. 11 Recycling results of the optimized LiBNi1 nanocomposites after 5 cycles of photocatalytic activity.

recycling photocatalytic test, removal proficiency fell slowly from 36.5% to 22.2%.

The following equations present the UV-degradation mechanism of acid red 88 contamination by optimal Li$_2$B$_4$O$_7$/NiO/Ni$_3$(BO$_3$)$_2$ nano-catalyst that has been shown in Schematic. 1:

$$Li_2B_4O_7/NiO/Ni_3(BO_3)_2 \text{ nano-catalyst } + h\nu$$
$$\rightarrow Li_2B_4O_7/NiO/Ni_3(BO_3)_2 * (e^-_{CB} + h^+_{VB})$$

$$O_2 + e^- \rightarrow {}^\bullet O_2^-$$

$$h^+ + H_2O \rightarrow {}^\bullet OH + H^+$$

$$H^+ + {}^\bullet O_2^- + e^- \rightarrow HOO^\bullet$$

$$HOO^\bullet + H_2O \rightarrow H_2O_2 + {}^\bullet OH$$

$${}^\bullet O_2^- + e^- + 2H^+ \rightarrow H_2O_2$$

$$H_2O_2 + e^- \rightarrow OH^- + {}^\bullet OH$$

$$OH^- + h^+ \rightarrow {}^\bullet OH$$

$$\text{Acid red 88 dye} + ({}^\bullet OH, {}^\bullet O_2^- \text{ or } h^+ \text{ active agents})$$
$$\rightarrow destruction products + H_2O + CO_2$$
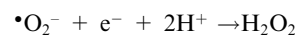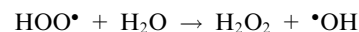
4. Conclusion

In summary, nano-scaled Li$_2$B$_4$O$_7$/NiO/Ni$_3$(BO$_3$)$_2$ composite samples were synthesized successfully by improved pechini sol–gel method in presence of starting materials of Ni(NO$_3$)$_2$·6H$_2$O, Li$_2$CO$_3$, H$_3$BO$_3$, ethylene glycol and EDTA complexing agent. The molar ratio of ethylene glycol:complexing agent:the sum of metal ions and types of complexing agents were examined adapted to the target of optimization of nanocomposite size and shape also, different types of complexing agents such as EDTA, citric acid, tannic acid, tartaric acid and phthalic acid were tested in pechini sol–gel route. Finally, photocatalytic performances of optimum Li$_2$B$_4$O$_7$/NiO/Ni$_3$(BO$_3$)$_2$ catalyst nanocomposites were studied for putting down of acid red 88 dye as

Fig. 10 Degradation percentage vs time of the optimized LiBNi1 nanocomposites in presence of three types of scavenger of benzoic acid, EDTA and Benzoquinone.
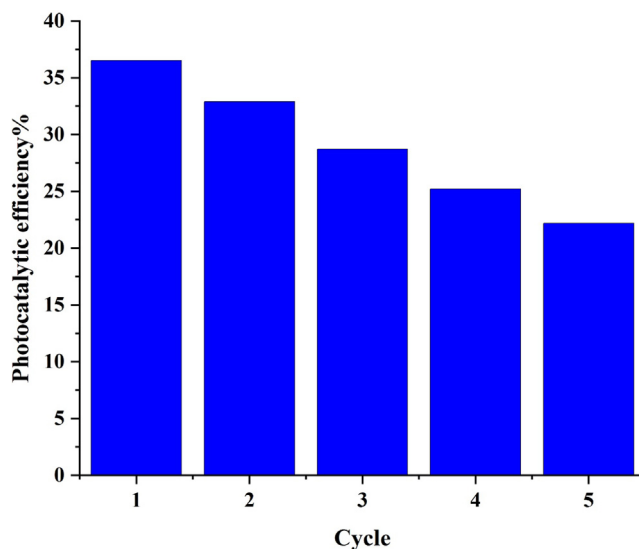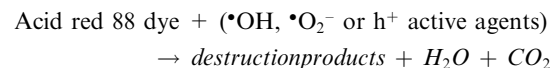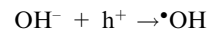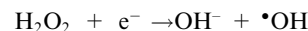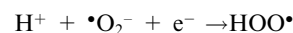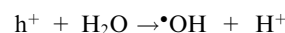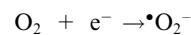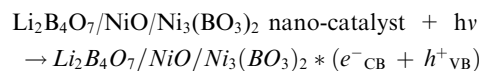
a water pollutant. LiBNi ternary nanocomposites with higher concentration have better photocatalytic efficiency under UV radiation (96.8%) than visible wave (36.5%).

CRediT authorship contribution statement

Makarim A. Mahdi: Investigation, Methodology, Formal analysis. **Layth S. Jasim:** Formal analysis, Software, Investigation, Writing – review & editing, Data curation. **Mahdi Ranjeh:** Investigation, Methodology, Formal analysis, Software. **Maryam Masjedi-Arani:** Writing – original draft, Formal analysis, Software, Writing – review & editing, Resources, Validation. **Masoud Salavati-Niasari:** Formal analysis, Methodology, Writing – review & editing, Writing – original draft, Conceptualization, Methodology, Supervision, Project administration, Investigation, Data curation.

Acknowledgements

References

Aadil, M., Rahman, A., Zulfiqar, S., Alsafari, I.A., Shahid, M., Shakir, I., Agboola, P.O., Haider, S., Warsi, M.F., 2021. Facile synthesis of binary metal substituted copper oxide as a solar light driven photocatalyst and antibacterial substitute. Adv. Powder Technol. 32, 940–950.

Ajeesha, T., Ashwini, A., George, M., Manikandan, A., Mary, J.A., Slimani, Y., Almessiere, M., Baykal, A., 2021. Nickel substituted MgFe2O4 nanoparticles via co-precipitation method for photocatalytic applications. Phys. B: Condens. Matter 606, 412660.

Al-Nayili, Albdiry, M., Salman, N., 2021. Dealumination of zeolite frameworks and Lewis acid catalyst activation for transfer hydrogenation. Arab. J. Sci. Eng. 46, 5709–5716.

Al-Nayili, Albdiry, M., 2021. AuPd bimetallic nanoparticles supported on reduced graphene oxide nanosheets as catalysts for hydrogen generation from formic acid under ambient temperature. New J. Chem. 45, 10040–10048.

Altin, I., Ma, X., Boffa, V., Bacaksız, E., Magnacca, G., 2021. Hydrothermal preparation of B-TiO2-graphene oxide ternary nanocomposite, characterization and photocatalytic degradation of bisphenol A under simulated solar irradiation. Mater. Sci. Semicond. Process. 123, 105591.

Arumugam, M., Choi, M.Y., 2020. Recent progress on bismuth oxyiodide (BiOI) photocatalyst for environmental remediation. J. Ind. Eng. Chem. 81, 237–268.

Arumugam, M., Yu, Y., Jung, H.J., Yeon, S., Lee, H., Theerthagiri, J., Lee, S.J., Choi, M.Y., 2021. Solvent-mediated synthesis of BiOI with a tunable surface structure for effective visible light active photocatalytic removal of Cr (VI) from wastewater. Environ. Res. 197, 111080.

Arumugam, M., Natarajan, T.S., Saelee, T., Praserthdam, S., Ashokkumar, M., Praserthdam, P., 2021. Recent developments on bismuth oxyhalides (BiOX; X= Cl, Br, I) based ternary nanocomposite photocatalysts for environmental applications. Chemosphere, 131054.

Bankole, P.O., Adekunle, A.A., Govindwar, S.P., 2018. Enhanced decolorization and biodegradation of acid red 88 dye by newly isolated fungus, Achaetomium strumarium. J. Environ. Chem. Eng. 6, 1589–1600.

Choura-Maatar, S., Nofal, M.M., M'nassri, R., Cheikhrouhou-Koubaa, W., Chniba-Boudjada, N., Cheikhrouhou, A., 2020.

Enhancement of the magnetic and magnetocaloric properties by Na substitution for Ca of La 0.8 Ca 0.2 MnO 3 manganite prepared via the Pechini-type sol–gel process. J. Mater. Sci.: Mater. Electron. 31, 1634–1645.

Dashairya, L., Sharma, S., Rathi, A., Saha, P., Basu, S., 2021. Solar-light-driven photocatalysis by Sb2S3/carbon based composites towards degradation of noxious organic pollutants. Mater. Chem. Phys. 273, 125120.

Fujioka, T., Ngo, M.T.T., Makabe, R., Ueyama, T., Takeuchi, H., Nga, T.T.V., Bui, X.-T., Tanaka, H., 2021. Submerged nanofiltration without pre-treatment for direct advanced drinking water treatment. Chemosphere 265, 129056.

Guo, Y., Li, C., Gong, Z., Guo, Y., Wang, X., Gao, B., Qin, W., Wang, G., 2020. Photocatalytic decontamination of tetracycline and Cr (VI) by a novel α-FeOOH/FeS2 photocatalyst: one-pot hydrothermal synthesis and Z-scheme reaction mechanism insight. J. Hazard. Mater. 397, 122580.

Guo, R.-F., Liang, P., Li, X.-Y., Liu, Z.-H., 2021. Fabrication of a dual Z-scheme GACN/NiO/Ni3 (BO3) 2 composite with excellent photocatalytic activity for methylene blue and tetracycline removal. Separ. Purif. Technol. 264, 118414.

Ighalo, J.O., Eletta, O.A., 2020. Recent advances in the biosorption of pollutants by fish scales: a mini-review. Chem. Eng. Commun., 1–12

Ji, M., Choa, Y.-H., Lee, Y.-I., 2021. One-step synthesis of black TiO2-x microspheres by ultrasonic spray pyrolysis process and their visible-light-driven photocatalytic activities. Ultrason. Sonochem. 74, 105557.

Kadhem, A., Al-Nayili, A., 2021. Dehydrogenation of formic acid in liquid phase over Pd nanoparticles supported on reduced graphene oxide sheets. Catal. Surv. Asia 25, 324–333.

Kambur, A., Pozan, G.S., Boz, I., 2012. Preparation, characterization and photocatalytic activity of TiO2–ZrO2 binary oxide nanoparticles. Appl. Catal. B: Environ. 115, 149–158.

Kim, S.B., Hong, S.C., 2002. Kinetic study for photocatalytic degradation of volatile organic compounds in air using thin film TiO2 photocatalyst. Appl. Catal. B: Environ. 35, 305–315.

Lu, Z., Chen, F., He, M., Song, M., Ma, Z., Shi, W., Yan, Y., Lan, J., Li, F., Xiao, P., 2014. Microwave synthesis of a novel magnetic imprinted TiO2 photocatalyst with excellent transparency for selective photodegradation of enrofloxacin hydrochloride residues solution. Chem. Eng. J. 249, 15–26.

Ma, X., Liu, X., Zhang, X., Piao, C., Liu, Z., Fang, D., Wang, J., 2021. Construction of dual Z-scheme NiO/NiFe2O4/Fe2O3 photocatalyst via incomplete solid state chemical combustion reactions for organic pollutant degradation with simultaneous hydrogen production. Int. J. Hydrogen Energy 46, 31659–31673.

Mahdiani, M., Soofivand, F., Ansari, F., Salavati-Niasari, M., 2018. Grafting of CuFe12O19 nanoparticles on CNT and graphene: eco-friendly synthesis, characterization and photocatalytic activity. J. Clean. Prod. 176, 1185–1197.

Masjedi-Arani, M., Salavati-Niasari, M., 2016. A simple sonochemical approach for synthesis and characterization of Zn2SiO4 nanostructures. Ultrason. Sonochem. 29, 226–235.

Mirzaei, M., Habibi, M.H., Sabzyan, H., 2021. Synthesis, characterization, and dye degradation photocatalytic activity of the nano-size copper iron binary oxide. Environ. Sci. Pollut. Res., 1–20

Nathan, R.J., Martin, C.E., Barr, D., Rosengren, R.J., 2021. Simultaneous removal of heavy metals from drinking water by banana, orange and potato peel beads: a study of biosorption kinetics. Appl. Water Sci. 11, 1–15.

Ramteke, D., Swart, H., Gedam, R., 2016. Spectroscopic properties of Pr3 + ions embedded in lithium borate glasses. Phys. B: Condens. Matter 480, 111–115.

Ranjeh, M., Masjedi-Arani, M., Salavati-Niasari, M., Moayedi, H., 2020. EDTA-modified sol-gel synthesis of monoclinic Li2MnO3 nanoparticles as an effective photocatalyst for degradation of organic dyes. J. Mol. Liq. 300, 112292.

Ranjeh, M., Masjedi-Arani, M., Amiri, O., Salavati-Niasari, M., 2021. Pechini sol-gel synthesis of Ni (II) doped LiMnBO3/Li2MnO3/Li2B2O4 nano-photocatalyst under UV–Vis irradiation. Int. J. Hydrogen Energy 46, 10324–10336.

Ranjeh, M., Amiri, O., Salavati-Niasari, M., Shabani-Nooshabadi, M., 2021. Preparation and study of characteristics of LiCoO 2/Fe3O 4/Li 2 B 2 O 4 nanocomposites as ideal active materials for electrochemical hydrogen storage. RSC Adv. 11, 23430–23436.

Rao, V.N., Ravi, P., Sathish, M., Reddy, N.L., Lee, K., Sakar, M., Prathap, P., Kumari, M.M., Reddy, K.R., Nadagouda, M.N., 2021. Monodispersed core/shell nanospheres of ZnS/NiO with enhanced H2 generation and quantum efficiency at versatile photocatalytic conditions. J. Hazard. Mater. 413, 125359.

Saravanan, A., Kumar, P.S., Vo, D.-V.-N., Yaashikaa, P.R., Karishma, S., Jeevanantham, S., Gayathri, B., Bharathi, V.D., 2020. Photocatalysis for removal of environmental pollutants and fuel production: a review. Environ. Chem. Lett., 1–23

Sayadi, M.H., Homaeigohar, S., Rezaei, A., Shekari, H., 2021. Bi/SnO 2/TiO 2-graphene nanocomposite photocatalyst for solar visible light–induced photodegradation of pentachlorophenol. Environ. Sci. Pollut. Res. 28, 15236–15247.

Seynnaeve, B., Folens, K., Krishnaraj, C., Ilic, I.K., Liedel, C., Schmidt, J., Verberckmoes, A., Du Laing, G., Leus, K., Van Der Voort, P., 2021. Oxygen-rich poly-bisvanillonitrile embedded amorphous zirconium oxide nanoparticles as reusable and porous adsorbent for removal of arsenic species from water. J. Hazard. Mater. 413, 125356.

Sharma, S., Bhattacharya, A., 2017. Drinking water contamination and treatment techniques. Appl. Water Sci. 7, 1043–1067.

Shen, L., Shi, Q., Zhang, S., Gao, J., Cheng, D.C., Yi, M., Song, R., Wang, L., Jiang, J., Karnik, R., 2021. Highly porous nanofiber-supported monolayer graphene membranes for ultrafast organic solvent nanofiltration. Sci. Adv. 7, eabg6263.

Tauc, J., Grigorovici, R., Vancu, A., 1966. Optical properties and electronic structure of amorphous germanium. Phys. Status Solidi (b) 15, 627–637.

Vitzthum, D., Schauperl, M., Strabler, C.M., Brüggeller, P., Liedl, K. R., Griesser, U.J., Huppertz, H., 2016. New high-pressure gallium borate Ga2B3O7 (OH) with photocatalytic activity. Inorg. Chem. 55, 676–681.

Wang, S., Zhao, L., Huang, W., Zhao, H., Chen, J., Cai, Q., Jiang, X., Lu, C., Shi, W., 2021. Solvothermal synthesis of CoO/BiVO4 pn heterojunction with micro-nano spherical structure for enhanced visible light photocatalytic activity towards degradation of tetracycline. Mater. Res. Bull. 135, 111161.

Zhang, C., Shi, J., Yang, X., De, L., Wang, X., 2010. Effects of calcination temperature and solution pH value on the structural and magnetic properties of Ba2Co2Fe12O22 ferrite via EDTA-complexing process. Mater. Chem. Phys. 123, 551–556.

Zhang, X., Tang, S., Du, Y., 2011. Synthesis and magnetic properties of antiferromagnetic Li2MnO3 nanoribbons. Phys. Lett. A 375, 3196–3199.

Zhang, Z., Wang, G., Li, W., Zhang, L., Guo, B., Ding, L., Li, X., 2021. Photocatalytic activity of magnetic nano-β-FeOOH/Fe3O4/biochar composites for the enhanced degradation of methyl orange under visible light. Nanomaterials 11, 526.

Zhu, Y., Wang, W., Yu, H., Wang, A., 2020. Preparation of porous adsorbent via Pickering emulsion template for water treatment: a review. J. Environ. Sci. 88, 217–236.